Supplement of The Cryosphere, 17, 1567–1583, 2023
https://doi.org/10.5194/tc-17-1567-2023-supplement
© Author(s) 2023. CC BY 4.0 License.

The Cryosphere Open Access EGU

Supplement of

Climatic control on seasonal variations in mountain glacier surface velocity

Ugo Nanni et al.

Correspondence to: Ugo Nanni (nanni@uio.no)

The copyright of individual parts of the supplement might differ from the article licence.

Contents of this file

Figures S1 to S9

Introduction

In this supplementary information, we provide details on the air temperature (Figure S1) measurements in our study area; on the temporal and spatial extent of the satellite imagery used in this study (Figures S2, S3, S4); on the method used to investigate the acceleration characteristics (Figures S5, S6); on the presence of debris and supraglacial ponds in our study area (Figure S7): on the velocities distribution on the ablation and accumulation zones (Figures S8, S9).

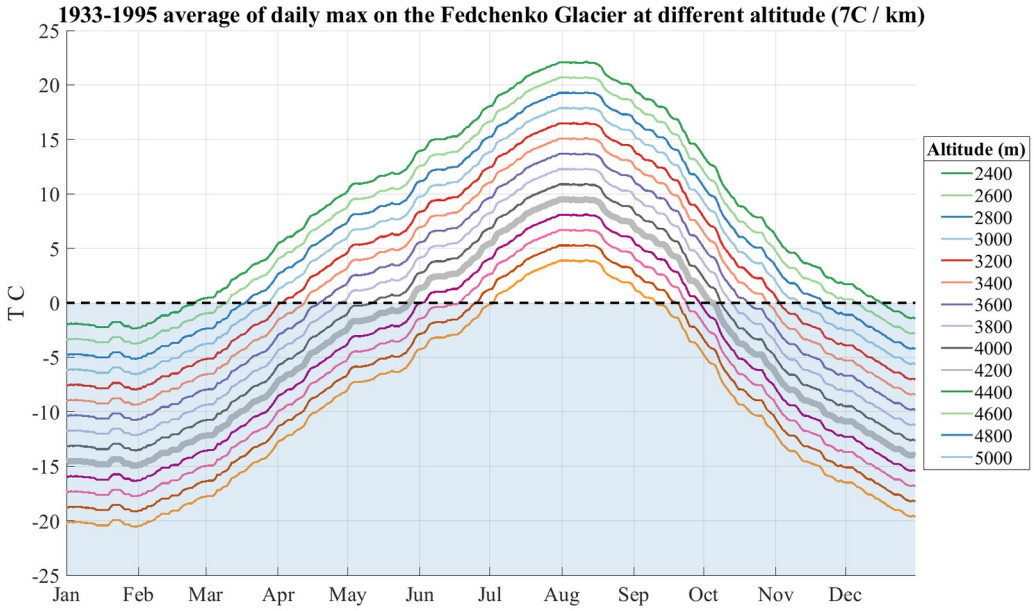

Figure S1. Daily maxima of air temperature at the Goburnov station on the Fedchenko glacier (4200 m elevation, see Lambretch et al., (2014)) averaged over the 63 years. Grey thick curve: average daily maximum in the air temperature measured. The other curves are shifted to given altitude with a lapse rate of 7C/km (Lambretch et al 2018). Blue shaded area shows negative temperature.

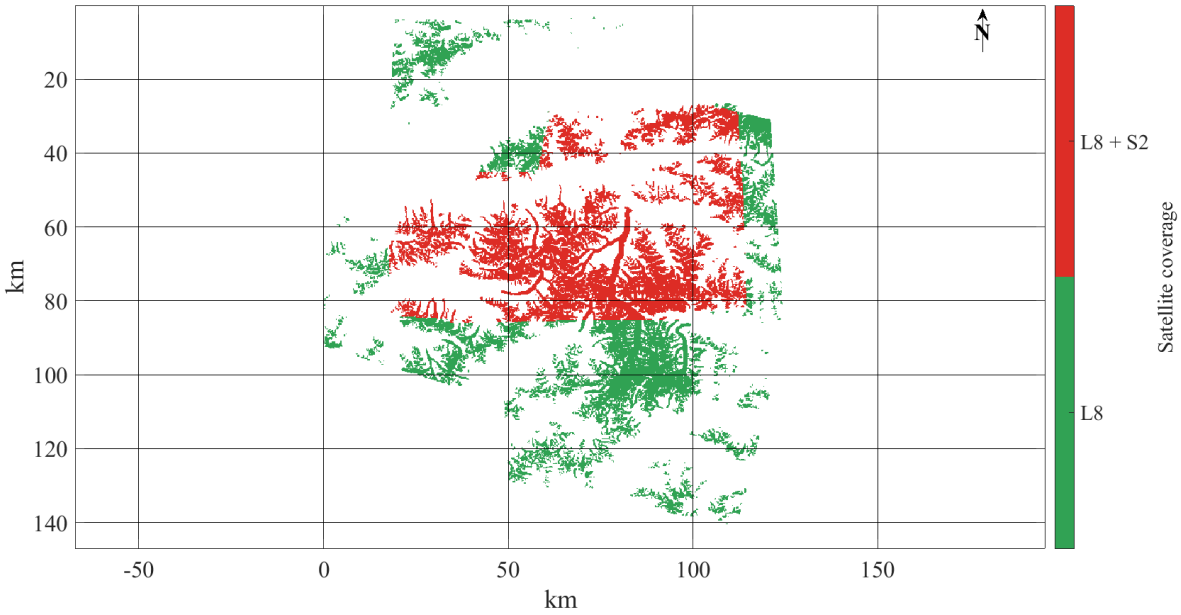

Figure S2. Spatial coverage of the selected tiles overlaid over the glacier contours from the Randolph Glacier Inventory (RGI Consortium, 2017). Within the red are, the glacier velocity fields are calculated with both Landsat 8 (L8) and Sentinel 2 (S2) tiles. Within the green are, the glacier velocity fields are calculated with Landsat 8 tiles only (L8).

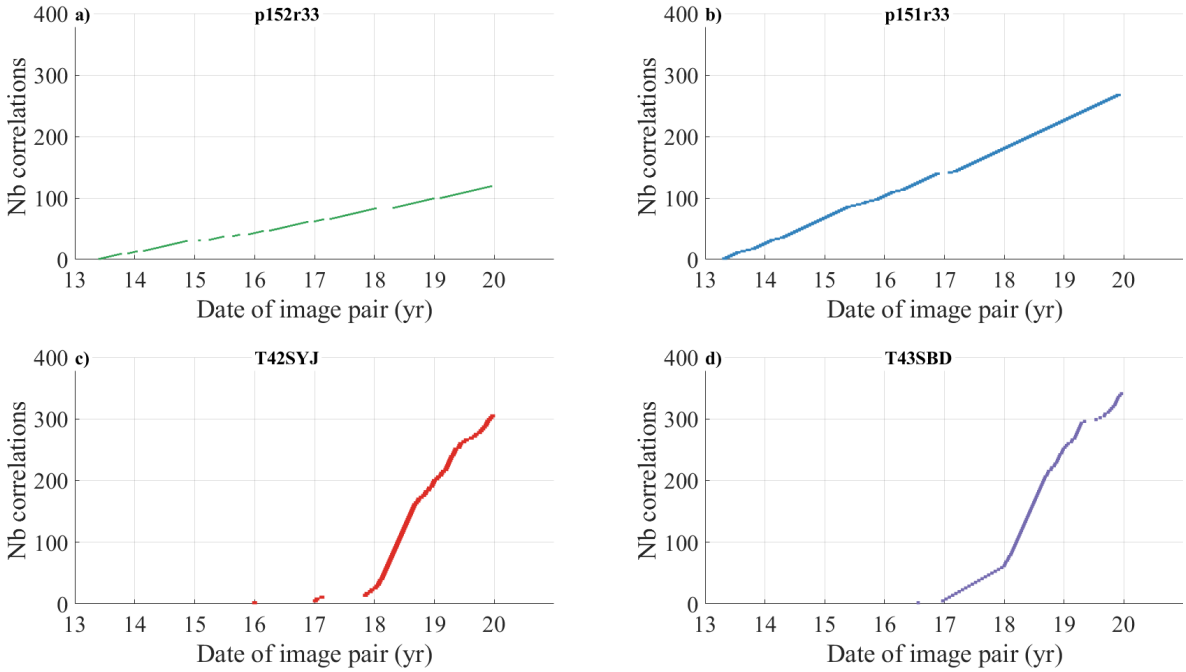

Figure S3. Cumulative number of correlation processed per tiles between 2013 and 2020. All pairs of 16 and 32 days are selected for Landsat 8 tiles (a, b). All pairs of 10, 20 and 30 days are selected for Sentinel 2 tiles. Image with cloud cover larger than 80% are excluded.

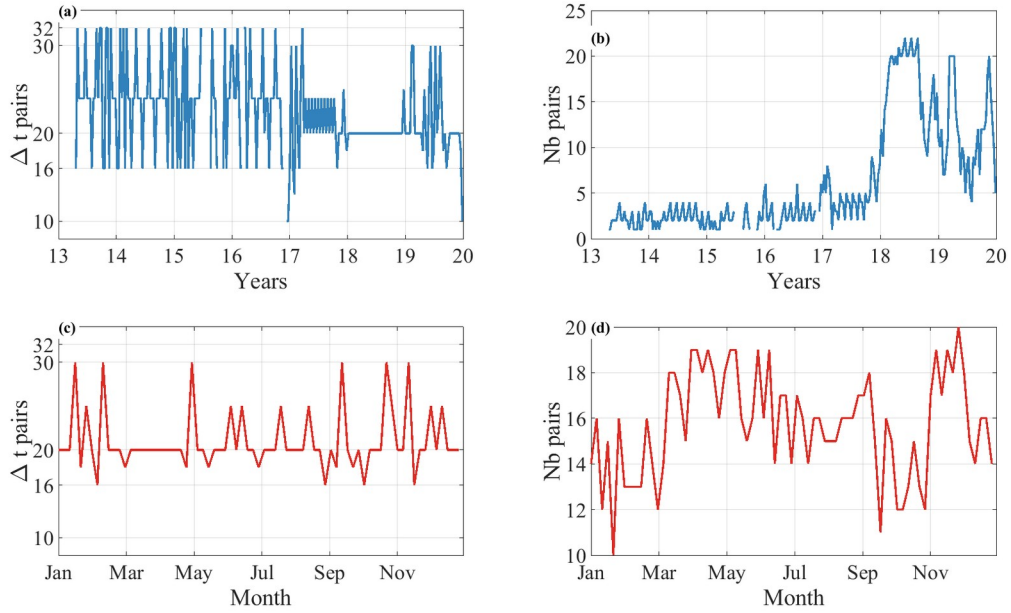

Figure S4. (a, c) Average time period between pairs of images as a function of time and (b, c) average number of pairs processed as a function of time.

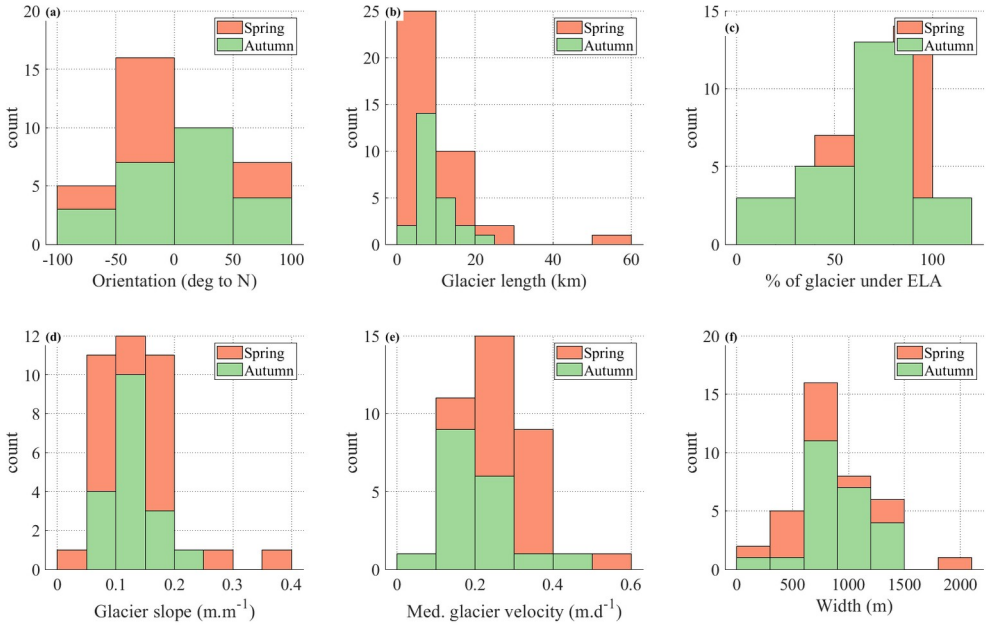

Figure S5. Characteristics of the glacier showing a spring/summer acceleration (red) and a the one showing an autumn acceleration (green). Glacier showing spring/summer acceleration are highlighted in Figure 1 of the main text.

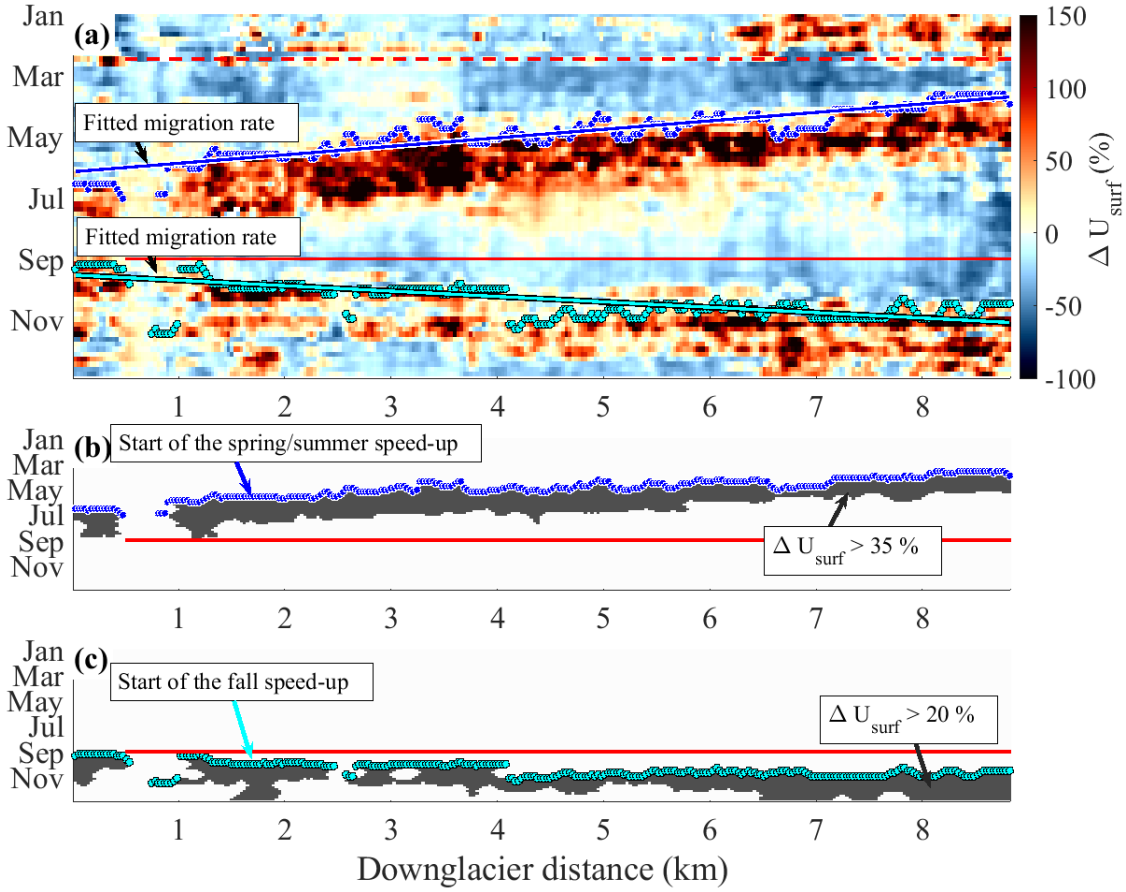

Figure S6. Illustration of the approach used to automatically pick the onset of the spring/summer and fall acceleration. (a) Background is the annual pattern of relative changes in glacier surface velocity with respect to the annual median velocity along the flowline of the Malyy Tanymas glacier (as in Figure 4 and Figure 5 of main text). Dark and light blue dots show automatically picked onset of the spring/summer and fall acceleration respectively. Dark and light blue lines show the linearly fitted migration of the acceleration onsets as a function of along flow distance. Dashed red line shows the initiation of the spring/summer period and plain red line of the fall period. (b, c) binary image showing in grey the values above 35% for spring/summer and 20% for autumn. In this binary image all components that are connected over a distance less than 1/5th of the glacier length in spring/summer and 1/10th in autumn are removed. See Section 4.3 for details.

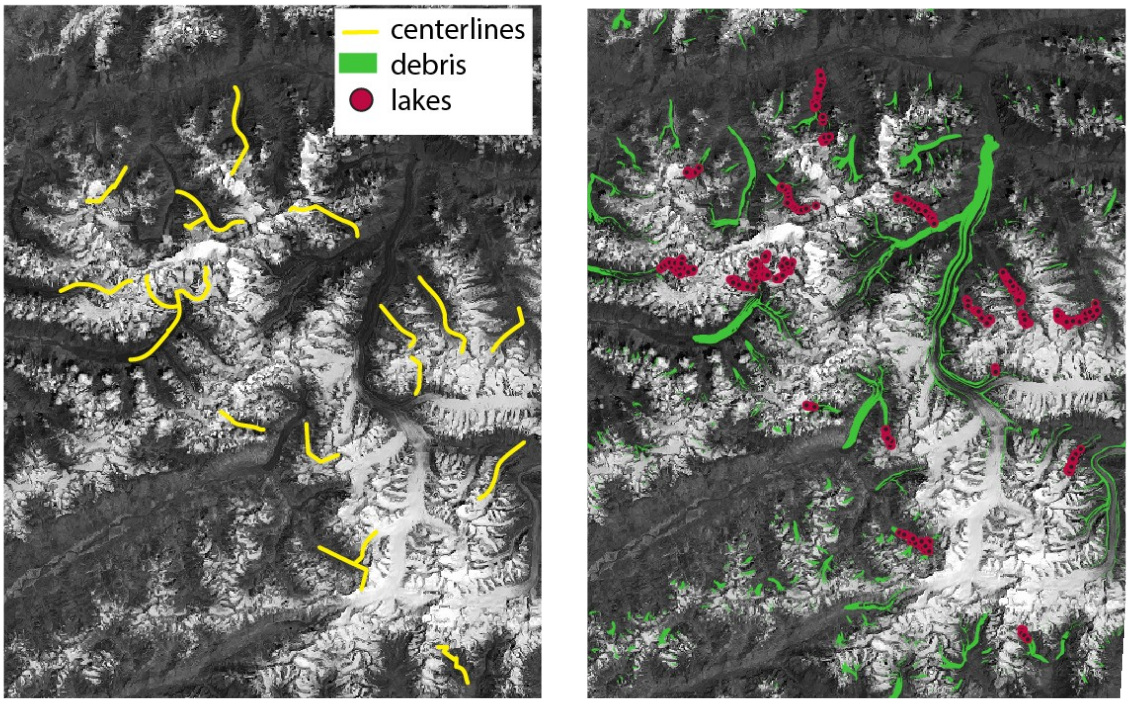
centerlines
debris
lakes

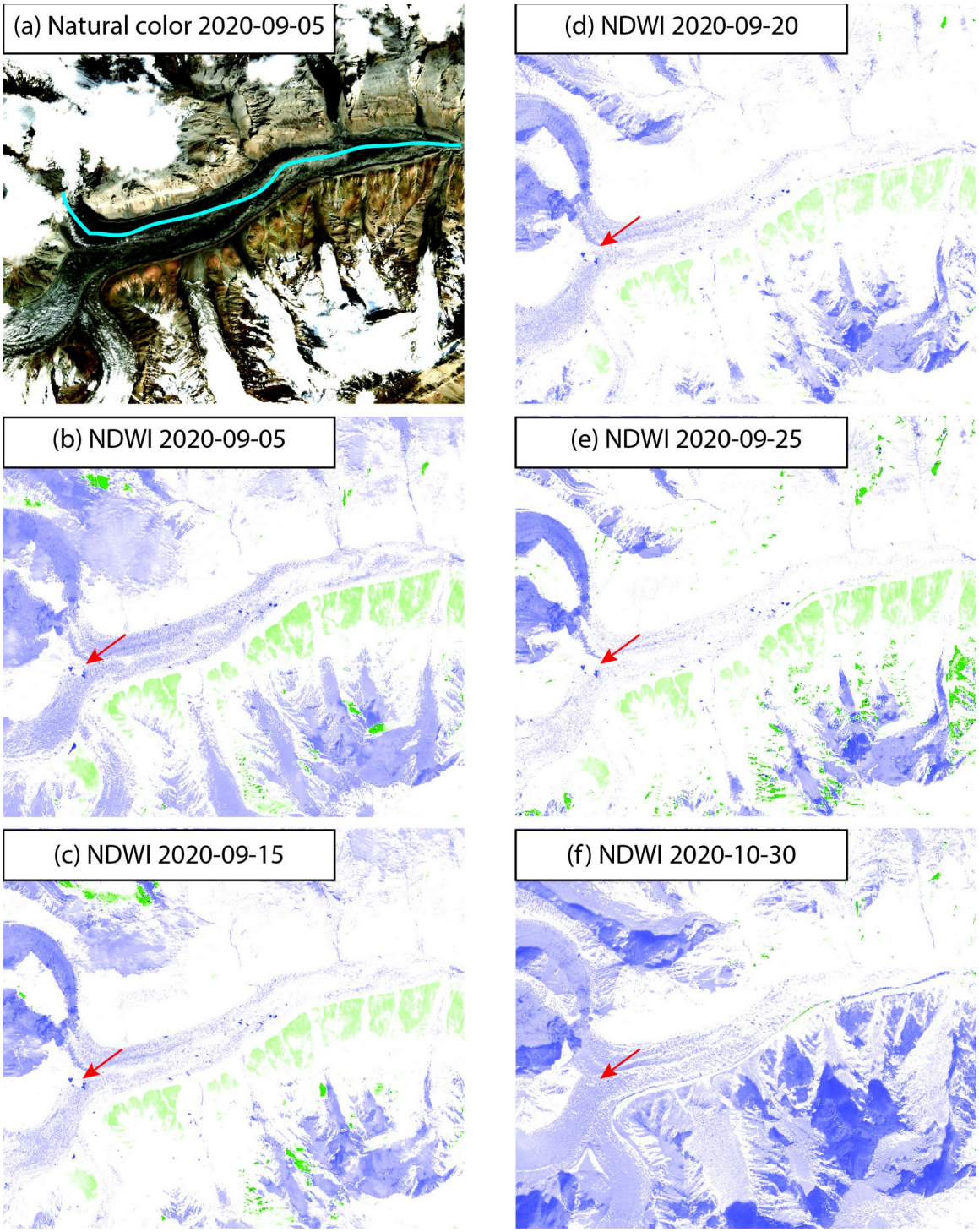

Figure S7. (Top figure) Manually mapped supraglacial ponds/lakes (red dots) using Planet basemap viewer (https://www.planet.com/) for the glaciers that presented an autumn acceleration (yellow lines). Debris cover map (green areas) is from Mölg et al., (2018). (Bottom figure) Close up to the MT glacier in September-October 2020. Images are provided by https://apps.sentinel-hub.com/sentinel-playground/. (a) Natural color image and centreline along which the velocity profiles are extracted. (b, c, d, e, f) Normalized Difference Water Index (NDWI) images. Red arrow show location of the upper lakes,

were the autmun acceleration has started. All images are snow-free. The different images show the presence of several lakes at the surface of the glacier and their disapereance in October. This could be due to frozen surface and/or lake drainage.

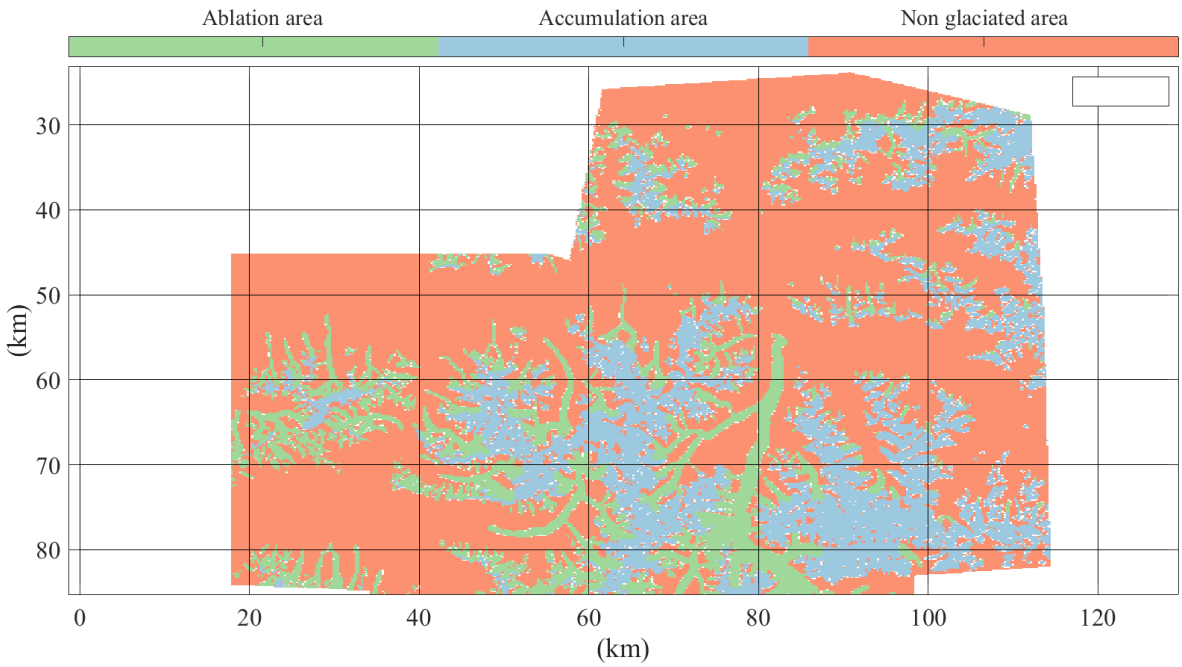

Figure S8. Delimitation of the studied areas used to calculate velocity distribution. Glacier contour is from the Randolph Glacier Inventory. The boundary between the accumulation and the ablation are is set at 4700m of elevation

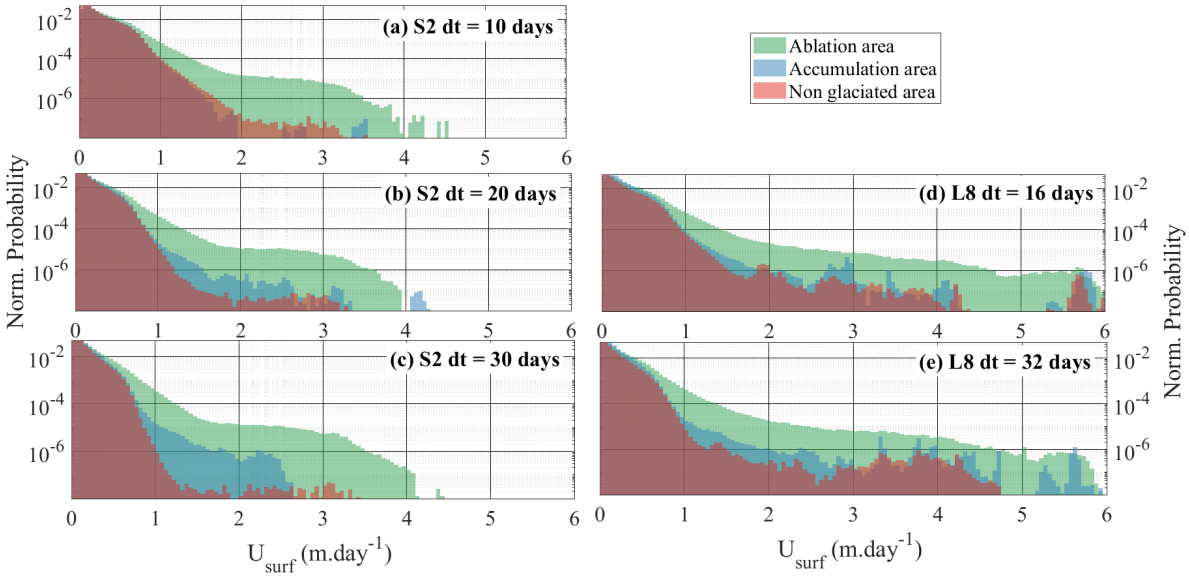

Figure S9. Distribution of the surface velocity over the ablation area, the accumulation area and the ice-free area (Figure S8) for the different sensors and time span dt between pairs. The distribution is computed only in the area where both Landsat 8 and Sentinel 2 tiles are used to calculate the velocity fields.

References:

Lambrecht, A., C. Mayer, A. Wendt, D. Floriciou, and C. Völksen. 2018. "Elevation Change of Fedchenko Glacier, Pamir Mountains, from GNSS Field Measurements and TanDEM-X Elevation Models, with a Focus on the Upper Glacier." *Journal of Glaciology* 64 (246): 637–48. https://doi.org/10.1017/jog.2018.52.

Lambrecht, Astrid, Christoph Mayer, Vladimir Aizen, Dana Floricioiu, and Arzhan Surazakov. 2014. "The Evolution of Fedchenko Glacier in the Pamir, Tajikistan, during the Past Eight Decades." *Journal of Glaciology* 60 (220): 233–44. https://doi.org/10.3189/2014JoG13J110.

Mölg, Nico, Tobias Bolch, Philipp Rastner, Tazio Strozzi, and Frank Paul. 2018. "A Consistent Glacier Inventory for Karakoram and Pamir Derived from Landsat Data: Distribution of Debris Cover and Mapping Challenges." *Earth System Science Data* 10 (4): 1807–27. https://doi.org/10.5194/essd-10-1807-2018.

RGI Consortium,2017.Randolph Glacier Inventory - A Dataset of Global Glacier Outlines, Version 6. Boulder, Colorado USA. NSIDC: National Snow and Ice Data Center. doi:https://doi.org/10.7265/4m1f-gd79